Influence of Field-Induced Phase Transition on Poly(Vinylidene Fluoride-Trifluoroethylene-Chlorotrifluoroethylene) Strain

P. Lheritier,[1,2,*] N. Vaxelaire,[1] S. Tencé-Girault,[3,4] F. Domingues Dos Santos,[5] and E. Defay[2,†]

[1] *Commissariat ă l'Energie Atomique, 17 Avenue des Martyrs, 38000 Grenoble, France*

[2] *Luxembourg Institute of Science and Technology, 5 Avenue des Hauts-Fourneaux, 4362 Esch-sur-Alzette, Luxembourg*

[3] *PIMM, Arts et Metiers Institute of Technology, CNRS, Cnam, HESAM University, 151 Boulevard de l'Hopital, 75013 Paris, France*

[4] *Arkema, CERDATO, Route du Rilsan, 27470 Serquigny, France*

[5]

This work is focused on understanding the reasons behind the large electrostrictive strain of poly(vinylidene fluoride-trifluoroethylene-chlorotrifluoroethylene) terpolymer. Although a few explanations have been proposed in the literature, it remains largely unclear. Here, the role of an electrically induced phase transition is investigated. The strain in the crystalline part of the polymer is monitored using XRD while an electric field is applied onto the sample. Three regions of interest are clearly evidenced and, of particular interest, we observe a change in crystal symmetry located on the 30–70 V μm^{-1} range. In that region, the lattice progressively loses its hexagonal symmetry and moves toward the phase usually observed at lower temperature, with a higher polar order. In parallel, we conduct macroscopic strain measurements to compare to the XRD data. Three different regimes are also observed with a sudden increase in electrostrictive coefficient on the 30–70 V μm^{-1} interval, going from 19 to 33 m^4 C^{-1}. This corresponds to a 1% strain, i.e., 25% of the total deformation measured at 100 V μm^{-1}. By thoroughly comparing macroscopic strain and x-ray measurements, we are able to single out and quantify the impact of this field-induced phase transition in the polymer overall strain.

I. INTRODUCTION

Electroactive polymers are promising candidates for applications such as sensors [1], actuators [2], or energy harvesters [3]. They are transparent, flexible, and less harmful to both health and environment than lead-based ceramics. Despite these interesting features, they struggle to reach the industrial market for two mains reasons: they require large driving fields and generate low mechanical stress compared to ceramics. In order to address these matters, many electroactive polymers have been developed over the past decades. Among the different candidates, poly(vinylidene fluoride-trifluoroethylene-chlorotrifluoroethylene) [P(VDF-TrFE-CTFE)] ter-polymer displays interesting performances, with strain up to 6% [4] for a Young modulus around 200 MPa [5]. In recent years, this polymer has been used as a matrix for inclusions [6], or blended with other materials [7] to further improve actuation performances. While these approaches are showing promising results, it appears that the origin of P(VDF-TrFE-CTFE) electromechanical performances is not fully understood. This work is an attempt to analyze quantitatively the mechanisms responsible for the P(VDF-TrFE-CTFE) large-strain response to an electric field.

The strain in PVDF-based polymers is commonly associated with their electrostrictive nature [8,9]. However, saying that a material is electrostrictive does not explain in any way the physical mechanisms at hand. It is merely a statement that the material strain follows the phenomenological law:

$$S = QD^2. \tag{1}$$

And, assuming the material is a linear dielectric:

$$S = Q(\epsilon E)^2 = ME^2, \tag{2}$$

*lheritier.p@gmail.com

†Emmanuel.defay@list.lu

where S is strain, Q is the electrostrictive coefficient, D is electric displacement, and ϵ is permittivity. S is the material strain, Q and M are its electrostrictive coefficients respective to the electric displacement (D) and electric field (E).

Numerous physical effects can induce an electrostrictive strain in a material. An overview of such mechanisms can be found in the work of Li *et al*. [10]. In the case of PVDF-based polymers, three mechanisms are likely to contribute to electrostriction: Maxwell strain, field-induced phase transition, and intrinsic electrostriction.

Maxwell strain is due to the Coulombian attraction between two surfaces with opposite charges. The attraction between the electrodes meets the mechanical resistance of the material, resulting in its compression [11]. Maxwell strain is often disregarded in PVDF and P(VDF-TrFE) [12] but not in terpolymers [13,14], due to their lower rigidity and higher permittivity than pure PVDF.

The second possible contribution to strain is an electric-field-induced phase transition [15,16]. In that case, the strain arises from the lattice difference between the two phases, and possibly domains alignment in the field direction. The existence of an electrically induced phase transition in P(VDF-TrFE-CTFE) is already established [17–19], although the different descriptions in the literature can appear confusing at times. The lattice symmetry of PVDF and its derivatives arise from how polymer chains are packed with respect to one another [20]. On the other hand, the ferroelectricity is a result of the chain packing but also of monomer conformation inside the chains. Sometimes, P(VDF-TrFE-CTFE) phases are assimilated to the α, β, γ phases of PVDF, based on their ferroelectric properties but regardless of the actual lattice symmetry [17,18]. To get a better understanding of the terpolymer structure, one can refer to Refs. [19,21]. For lack of a better expression, we also refer to the electric-field-induced change as a phase transition, toward a phase with a higher ferroelectric order.

Finally, intrinsic electrostriction relates to how the displacement of charges in a crystal can induce a macroscopic strain [10]. It is worth mentioning that from an engineering point of view, there is no need to discriminate the contributions of different mechanisms, as they all combine into a single electrostrictive coefficient. Still, in order to develop new materials with large electrostrictive strain, we need to understand what the key mechanisms are.

In this work we measure simultaneously the polarization and strain of P(VDF-TrFE-CTFE) samples. On a localized polarization range, we observe a nonlinear electrostrictive behavior. This allows us to single out and quantify the contribution of a specific mechanism. Using XRD on samples submitted to a dc field, we link this additional strain to changes in the crystalline structure, the so-called phase transition. We successfully quantify the contribution of this mechanism to the electrostrictive performances of P(VDF-TrFE-CTFE).

II. METHOD AND CHARACTERIZATIONS

The P(VDF-TrFE-CTFE) (61/31/8%) is provided by Piezotech-Arkema as powder. It is dissolved in cyclopentanone for 24 h while stirring at 90 °C, resulting in an homogeneous paste. This paste is used as an active layer of a fully screen-printed capacitor. Top and bottom electrodes are made of poly(3,4-ethylenedioxythiophene) polystyrene sulfonate (PEDOT:PSS) purchased from Hereaus and stirred for 15 min at room temperature before use. Two different types of substrate are used: thick amorphous glass for XRD characterization and 125-μm-thick polyethylene naphthalate (PEN) films for strain and polarization measurements.

Each PEDOT:PSS layer is annealed at 115 °C for 5 min after deposition. The annealing of the active layer is divided in two steps: first 5 min at 60 °C in order to evaporate the solvent, followed by a second step at 115 °C for 15 min. The active layer thickness is measured using a profilometer, with typical values around 1 μm. After this, the cantilevers are cut out from the PEN substrate with a laser.

Figure 1 sketches one polymer device with the measurement principle for strain and polarization measurements. We use a chromatic confocal sensor with submicron resolution (STIL Initial) to measure device deflection. Polarization P versus electric field E (P-E loops) are acquired with a Radiant precision premier tester. The waveform we use to get the polarization is also the driving signal for the actuation measurement. A triggering pulse is sent from the Radiant tester to the confocal sensor in order to synchronize both measurements. As a result, we obtain the device deflection as a function of its polarization.

The material strain is calculated from the beam deflection using Eq. (3), simplified from Ref. [5], provided that $t_p \ll t_s$ and $Y_p < Y_s$.

$$\delta = \frac{3 t_p L^2}{Y_s t_s^2} Y_p S_1. \tag{3}$$

The subscripts s and p refer, respectively, to substrate and polymer. Y is the Young modulus and t layer thickness. L is beam length, and δ the measured deflection. S is the terpolymer strain, the subscript 1 denotes an in-plane strain direction, perpendicular to applied electric field. Values for Young's modulus are taken from the PEN manufacturer's data and from Ref. [22]. The typical dimensions for the entire device are 20 mm × 4 mm × 128 μm.

The XRD study is performed on a Panalytical-EMPYREAN® two-circle diffractometer in Bragg-Brentano configuration using a Cu anode ($\lambda = 1.5406$ Å) as the source. Spectra are recorded in a symmetrical coplanar geometry (or Theta/2Theta geometry). Therefore, crystallites are probed in the out-of-plane (or z) direction corresponding to the electric field direction. During *in situ* biasing measurement, x-ray beam is reduced to few mm

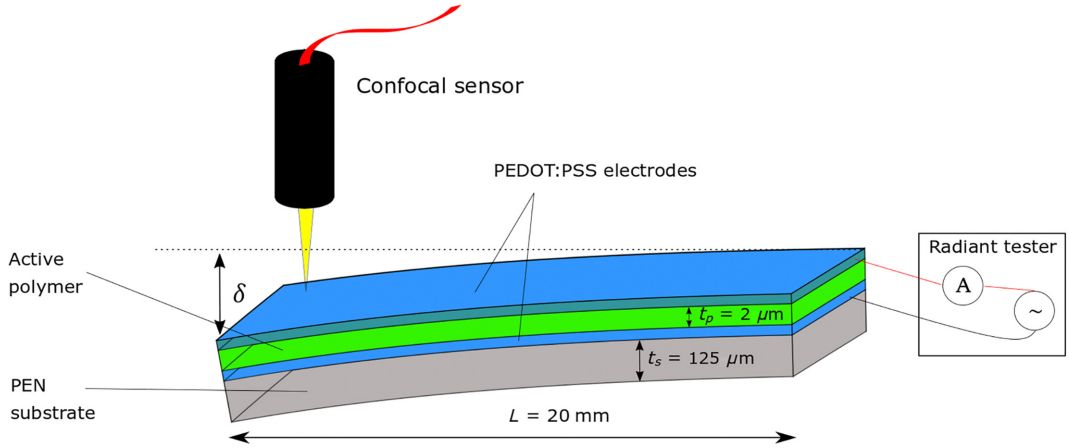

FIG. 1. Sketch of the heterogeneous cantilever (PEN substrate/PEDOT:PSS/terpolymer/PEDOT:PSS) and the measurement setup allowing for collecting polarization versus electric field (Radiant tester) and mechanical deflection versus electric field.

to shot at the center of the 20-mm circular capacitor and avoid border effect. In order to reduce the acquisition time to reasonable durations we limit the measurements to a 2.5° range using one-dimensional Pixel® detector in scanning mode. The angle is confined between $2\theta = 17.2°$ and $2\theta = 19.7°$, where the terpolymer main diffraction peak is located. The complete XRD spectrum of a terpolymer sample is shown within the Supplemental Material [23]. The need to shorten the measurement duration is driven by the increased risk of failure of a sample submitted to high dc field for a long period. The electric bias is applied through contact needles driven by a Keithley® 2635B source and measurement unit. Electrical integrity of the sample is tested before and after *in situ* dc biasing. Prior to measurements, capacitor radiation endurance is validated during one-night x-ray exposition where no change in peak is observed.

III. RESULTS

The P(VDF-TrFE-CTFE) polarization and strain responses to an electric field up to 20 V μm^{-1} are displayed in Fig 2.

In Fig. 2(a), the polarization cycle corresponds to that of a linear dielectric material, which can be fitted by a relative permittivity ϵ_r of 29.5. The opening in the cycle is due to the dielectric losses and the lag they induce in the polarization response. Figure 2(b) shows the strain measured as a function of electric field, with a parabolic fit corresponding to an electrostrictive coefficient $M = 1.3\ 10^{-18}$ m^2 V^{-2} [Eq. (1)]. Combining the data in Figs. 2(a) and 2(b), strain is plotted versus squared polarization in Fig. 2(c). A linear fit of the strain gives an electrostrictive coefficient $Q = 19$ m^4 C^{-2} [Eq. (2)].

This measurement procedure is repeated for higher electric field values, up to 120 V μm^{-1}, with the results displayed in Fig. 3.

Figure 3(a) shows the polarization cycle up to 120 V μm^{-1}. The cycle is highly nonlinear and displays the characteristic double hysteresis loop of P(VDF-TrFE-CTFE) terpolymer derivatives [19]. In Fig. 3(b), the strain versus electric field also displays a hysteresis loop, up to 70 V μm^{-1} where the loop closes. Figure 3(c) combines Figs. 3(a) and 3(b) with the strain versus squared polarization for the unipolar cycle lower branch. The full cycle

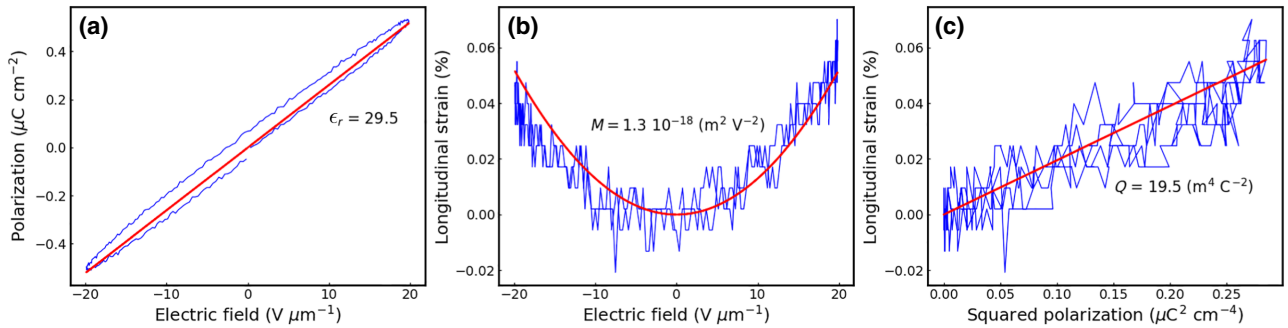

FIG. 2. (a) Polarization cycle of the terpolymer at 1 Hz and 20 V μm^{-1} and the linear fit corresponding to $\epsilon_r = 29.5$. (b) Simultaneous strain measurement, fitted with Eq. (2). (c) Strain from (b) plotted against squared polarization and fitted with Eq. (1).

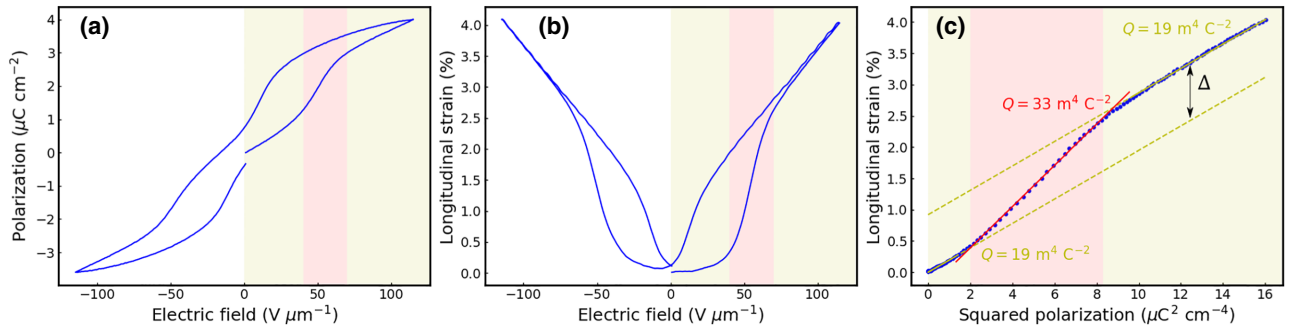

FIG. 3. (a) Polarization cycle of the terpolymer at 1 Hz and 120 V μm^{-1} (b) Simultaneous strain measurement. (c) Unipolar strain lower branch in (b) plotted against squared polarization and fitted with Eq. (1). The colored background is a visual aid for the discussion below.

can be found within the Supplemental Material [23], but is not represented here for the sake of clarity.

In Figs. 3(a) and 3(b) polarization and strain show a non-linear behavior. Consequently, Eq. (2) becomes irrelevant and neither permittivity ϵ_r nor electrostrictive coefficient M can be obtained as we did for low electric field measurements. In Fig. 3(c), however, an interesting behavior is displayed: on three separate intervals, the strain is linear with regard to the squared polarization. For each interval, an electrostrictive coefficient Q can be calculated with Eq. (1). These Q values and the linear fits are displayed on the graph and in Table I. The red background in all three graphs corresponds to the interval where Q equals 33 m^4 C^{-2}. The electric field, polarization and electrostrictive coefficient values of each interval are also regrouped in Table I.

Together with macroscopic strain measurements, we observe the evolution of the crystalline phase with electric field. We measure the XRD spectra of a terpolymer sample at different dc field values; Fig. 4 displays the resulting scans. The signal intensity is provided in arbitrary units as a function of the angle 2θ. The 2θ angle is the angle between incident and diffracted wavevector. In symmetrical geometry, incident and emergent angle are equal to $2\theta/2$. The θ angle is the one using Bragg's law $\lambda = 2d\sin(\theta)$.

In Fig. 4(a), the XRD spectra are measured for electric field values ranging from 0 to 17 V μm^{-1}. On this interval, the XRD diffraction peak displays no significant evolution in position or shape. The spectra in Fig. 4(b) are acquired for electric field values between 23 and 71 V μm^{-1}. As the electric field increases, the diffraction peak becomes more intense, thinner, and the asymmetry switches from left to right. Figure 4(c) displays XRD patterns for electric fields up to 166 V μm^{-1}. At higher electric fields, the diffraction peak goes towards higher 2θ values while maintaining an almost identical shape.

TABLE I. Electric field intervals corresponding to the break in the linear P^2 fit displayed in Fig. 3(c), with the corresponding electrostrictive coefficients Q.

E (V μm^{-1})	P^2 (μC^{-2} cm^{-4})	Q (m^4 C^{-2})
[0; 40]	[0; 2]	19
[40; 70]	[2; 8.3]	33
[70; 120]	[8.3; 16]	19

The diffraction peak observed Fig. 4 and recorded in a narrow 2θ range correspond to the main peak of the relaxor ferroelectric (RFE) crystal structure [21,24]. The integrated intensity and the full width at half maximum of this diffraction peak are reported Fig. 5(a). We observe a thinning of the peak and an increase in intensity when the applied electric field increases, this behavior is reversible and hysteretic. As we discuss later and thanks to Refs. [21,24] we interpret this asymmetrical peak as the juxtaposition of two Bragg peaks associated with the (200) and (110) planes of the orthorhombic RFE crystal phase.

Thus, over the whole electric field range, the diffraction peak can be fitted with two pseudo-Voigt functions, the first one located at around 18° is associated with the d_{200} interplanar distance while the other one is attributed to the d_{110} distance. Three fit examples are displayed in Figs. 4(d), 4(e), and 4(f) at 0, 29, and 119 V μm^{-1}, respectively. The fits of all spectra are performed in a single run [25]: the boundary conditions and initial parameters are identical throughout the operation (Supplemental Material [23]). The fit displayed in Figs. 4(d) is similar for all other spectra in Fig. 4(a). The fit in Fig. 4(e) illustrates what happens in Fig. 4(b): the main evolution appears on intensities, peak 2 becomes gradually more intense while peak 1 shrinks.

In Fig. 4(c), the fits are similar to Fig. 4(f), the position shifts towards higher 2θ. For all the refinements, the width of the two Bragg peaks (200) and (110) remains constant for any value of applied electric field.

Using the data from Fig. 4, we calculate the integrated intensity of each peak [Fig. 5(c)] and convert the 2θ values using Bragg's law to get their respective interplanar distances, d_{200} and d_{110}, displayed in Fig. 5(b).

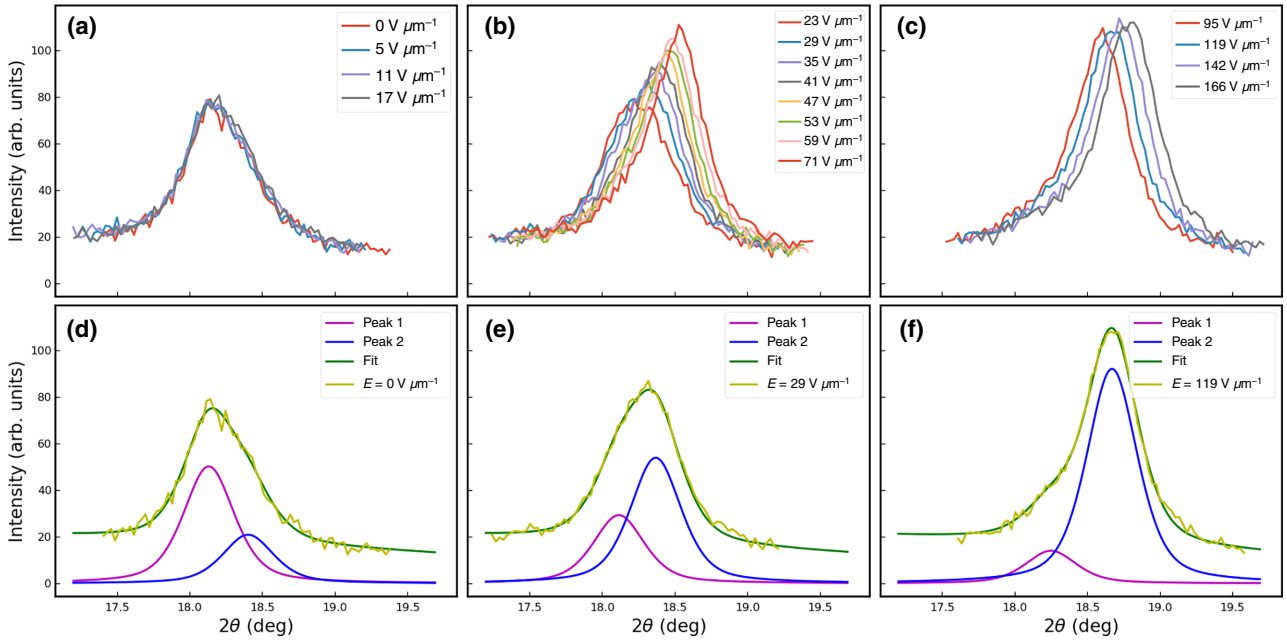

FIG. 4. Raw spectra of the terpolymer under electric field. The data are separated into three panels based on the range of electric field applied. (a) 0–17 V μm^{-1}. (b) 23−71 V μm^{-1}. (c) 95−166 V μm^{-1}. (d)–(f) fit with the same two pseudo-Voigt functions.

In Fig. 5(c) the integrated intensities are normalized with respect to the total area at zero field. This graph shows quantitatively the evolution already visible in Fig. 4. The integrated intensity of the (110) peak increases, at the expense of the (200) peak intensity. The evolution is slightly hysteretic and mostly located on the 30–65 V μm^{-1} electric field range. Note that the total area [Fig. 5(a)] is not constant with electric field, meaning a change in the amount of crystalline domains fulfilling Bragg's condition, this change is reversible when electric field decreases.

In Fig. 5(b), the decrease in interplanar distance corresponds to a negative out-of-plane strain, as opposed to the in-plane strain measurements in Figs. 3 and 4. This is due to the Bragg-Brentano configuration probing dimensions in the same direction as the electric field and not perpendicular to it. At zero field, the first diffraction peak correspond to d_{200} around 4.77 Å and the second one to d_{110} around 4.70 Å. Up to 30 V μm^{-1}, the two peaks keep the same positions and their intensities remain constant. Between 30 and 65 V μm^{-1}, d_{110} decreases to 4,67 Å while d_{200} remains constant at 4.77 Å, in this range the intensity I_{110} increases at the expense of I_{200}. For electric field higher than 70 V μm^{-1} the two d spacings decrease simultaneously while the intensities of the two diffractions remain constant. These jumps of 0.05 and 0.1 Å for d_{200} and d_{110} corresponds, respectively, to strain variations of 1 and 2%.

IV. DISCUSSION

Figure 2(c) confirms the electrostrictive nature of P(VDF-TrFE-CTFE), with a strain response showing a quadratic dependence with polarization. Since the terpolymer is also a linear dielectric [Fig. 2(a)], it results in a quadratic dependence to the electric field [Fig. 2(b)]. Strain and M coefficient have values of the same order but lower than similar reports [26]. This can be due to an overestimation of the material rigidity [Eq. (3)], or lower performances due to a difference in the fabrication process [22,27].

As electric field increases, the polarization cycle of P(VDF-TrFE-CTFE) becomes hysteretic and nonlinear [Fig. 3(a)]. This is commonly associated with a combination of the terpolymer relaxor nature [24] and the electrically induced phase transition [28]. On the other hand, the strain-cycle double-hysteresis loop in Fig. 3(b) has scarcely been investigated. Of particular interest, the representation in Fig. 3(c) shows a rupture in the electrostrictive behavior of the terpolymer. On a localized electric field range (40–70 V μm^{-1}) the coefficient Q sharply increases from 19 to 33 m^4 C^{-2} then goes back to its previous value. The corresponding increase in strain is noted Δ in Fig. 3(c) and is worth about 1%. At 100 V μm^{-1} the total longitudinal strain is 4%. Therefore, this "jump" amounts to about 25% of the total macroscopic strain. This measurement is reproduced on another sample with similar results (Supplemental Material) [23].

Having isolated and quantified a single electrostrictive mechanism, we need to identify it. Out of the different possibilities described in the Introduction, the so-called electric-field-induced phase transition is the most likely explanation. Indeed, there is no reason for intrinsic electrostriction nor Maxwell strain to appear only at a

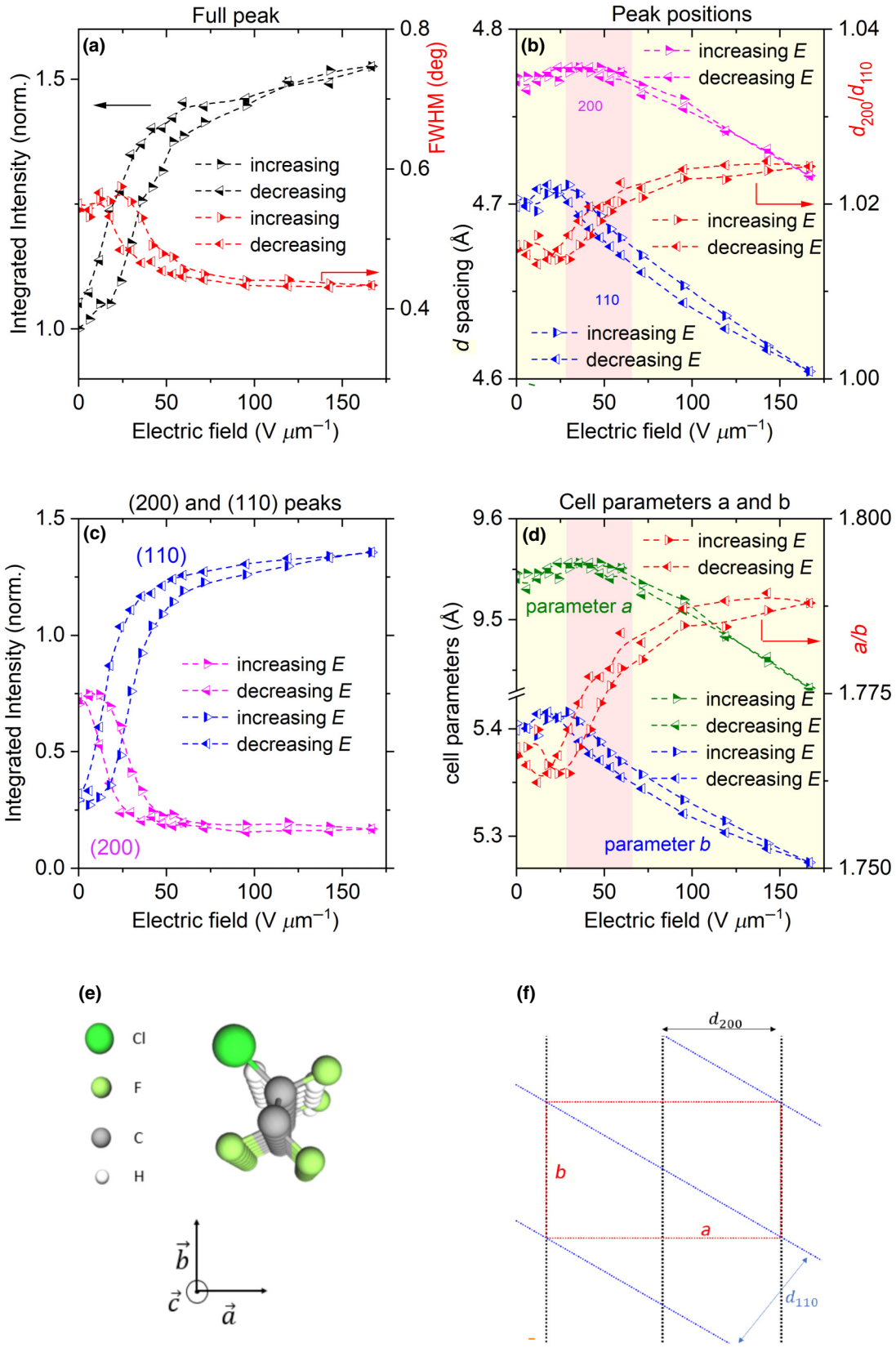

FIG. 5. (a) Normalized integrated intensity and full width at half maximum of the full asymmetric peak, (b) *d* spacing of the two fitting Bragg peaks, (c) normalized integrated intensity of the (200) and (110) fitting peaks, and (d) *a* and *b* cell parameters deduced from the fitting, as a function of electric field. (e) Schematic representation of polymer chain along the c axis. (f) Representation of the crystal unit cell.

certain voltage then disappear just as abruptly. The phase transition can only occur in the crystalline phase, which makes XRD the best tool to test this hypothesis. As already explained and in agreement with the literature [21,24], the diffraction line recorded in our restrained 2θ range correspond to the (200) and (110) diffraction planes of the orthorhombic pseudo hexagonal RFE crystal phase of the P(VDF-TrFE-CTFE). The associated d spacing, d_{200} and d_{110}, can be expressed as function of cell parameters a and b [29].

$$d_{200} = {}^{a}/_{2} \quad \text{and} \quad d_{110} = {}^{1}\Big/\sqrt{\left(\tfrac{1}{a^2} + \tfrac{1}{b^2}\right)}.$$

With these expressions, we deduce the evolution of cell parameters a and b with the applied electric field. These data are reported in Fig. 5(d), along with the a:b ratio. This ratio is equal to $\sqrt{3}$ for the high-temperature hexagonal PE crystal phase [21,24,29]. Again, in Fig. 5(d), we observe three domains for the evolution of the cell parameters with the applied electric field. For low electric field, lower than 30 V μm^{-1}, no evolution of the cell parameters is detected, we observe only a small increase of I_{110} and a decrease of I_{200}. We interpret this evolution as an increase of the (110) planes in Bragg's condition, parallel to the sample surface, at the expense of (200) planes, it corresponds to a slight orientation of the dipoles parallel to the electric field without change in the crystal cell. For these low electric fields, we measure $a = 9.55$ Å, $b = 5.41$ Å, leading to a:$b = 1.76$. For an electric field higher than 30 V μm^{-1} and lower than 65 V μm^{-1}, the orientation of the dipoles continues (increase of I_{110} and decrease of I_{200}), Fig. 5(c), along with a significant decrease of b parameter keeping the cell parameter a constant. For this electric field domain, the ratio a:b increase from 1.76 to 1.78. Afterwards, for electric field higher than 70 V μm^{-1}, the orientation of the dipoles does not evolve more, the intensities of the Bragg peaks remain constant, the two cell parameters decrease when the applied electric field increases. For the high electric field domain (E > 100 V μm^{-1}), the ratio a/b is constant around 1.79. All these evolutions are reversible with small hysteresis, thus changes in the XRD spectra are due to dipole alignment in the applied electric field direction without crystallinity changes. The applied electric field induces also a change in the cell parameters, a and b, leading to a change of the ratio a:b. This ratio evolves mostly for electric field between 30 and 100 V μm^{-1} [Fig. 5(d)], it corresponds to a change of the crystal cell shape. For high electric field the crystal cell is pseudohexagonal but less and less «hexagonal» and conversely for weak electric field, the pseudohexagonal cell is more and more «hexagonal», a:b ratio evolves towards $\sqrt{3}$. Figure 6 is a schematic representation of the crystalline unit cell at different applied electric fields. The aim is to provide a visual support for the discussion above and for that purpose the changes are not to scale.

In Fig. 6, the symmetry changes from hexagonal to orthorhombic, hence the term field-induced phase transition. This is a simplification, as the symmetry is only hexagonal for the high-temperature paralectric phase. At room temperature, the terpolymer is in between two phases: the low-temperature, orthorhombic, RFE phase, and the high-temperature, hexagonal, PE phase [21]. The electric field pushes the structure toward that of the low-temperature orthorhombic phase.

The first point of interest is the qualitative behavior observed in both measurements. Similar to the cantilever

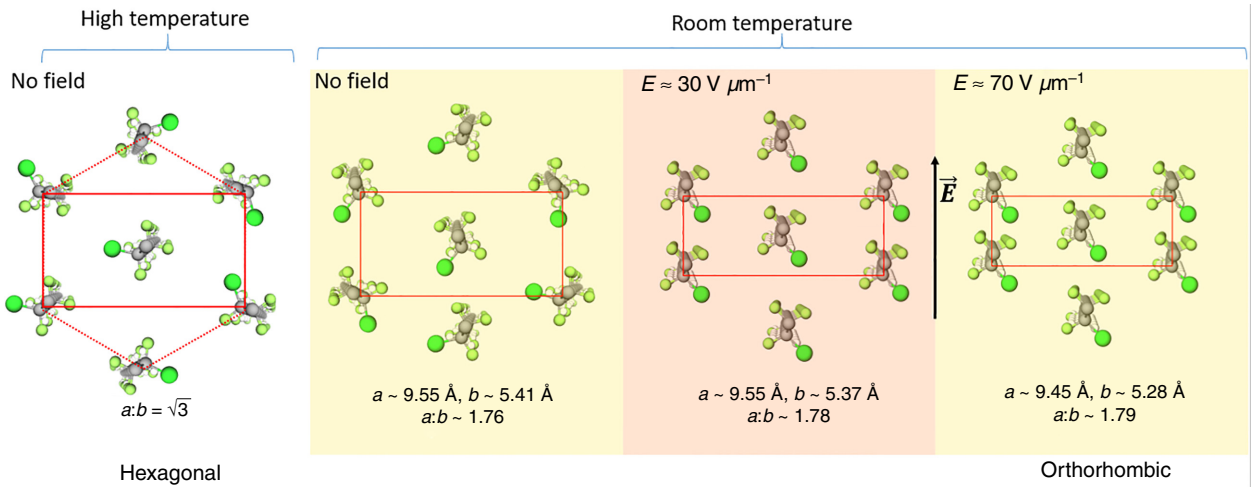

FIG. 6. Schematic representation of the unit-cell parameters as a function of the applied electric field. The left panel represents the high-temperature state without field, where the lattice symmetry is hexagonal. With the application of an electric field the lattice is further distorted and ends up orthorhombic, as represented on the middle-right and right panels. The color coding for the three regimes is the same as in Figs. 3 and 5.

strain, the XRD response can be separated into three intervals. Said intervals are highlighted by the colored background in Figs. 3 and 4. It appears that both the change in crystal shape (a:b ratio) and the increase in electrostrictive coefficient Q occur on the same electric field range. Consequently, we consider that the so-called "field-induced phase transition" is responsible for this particular electrostrictive contribution. The small quantitative discrepancies in terms of electric field intervals between the two measurements are ascribed to the frequency dependence of terpolymer response. Indeed, the XRD cycle is acquired at a much lower frequency than the cantilever one, respectively 2.10^{-4} Hz and 1 Hz. The polarization curves showing the terpolymer frequency dependence are available within the Supplemental Material [23].

Going further, we can estimate how much this effect weight in each measurement. Starting with the XRD patterns, the b parameter is measured at 5.41 Å at zero field and 5.33 Å at 100 V μm^{-1}. About 50% of this variation occurs at constant value of the a parameter and therefore corresponds to the change in crystal symmetry. Comparatively, the macroscopic increase in electrostrictive coefficient only amounts for 25% of the total strain measured at 100 V μm^{-1} [Δ in Fig. 3(c)]. The variations are much smaller than what is observed in the crystal. This is consistent with field-induced transition as the origin of increased electrostrictive response. The crystalline part of terpolymer undergoes large strain variations, but since it makes up for only 30 to 50% [22] of the total volume, it is less visible macroscopically.

This discussion is focused on the changes in peak position with the electric field and not on the change in intensity [Figs. 5(a) and 5(c)]. This is because the variation in intensity can be caused by different mechanisms, which are difficult to separate from one another. Such changes may be related to an increase of the sample crystallinity when an electric field is applied. They can also be due to texturing effects, since the peak intensity depends on the amount of crystalline planes verifying Bragg's condition. The application of an electric field in the terpolymer creates a preferential orientation of dipoles that change the crystalline planes' orientation, making the polymer anisotropic. Then, diffraction planes presenting dipoles parallel to the electric field become more represented. In that scenario, the (110) peak intensity should increase at the expense of the (200) one, as observed, regardless of the unit-cell parameters. In ceramic, electrically induced anisotropy could come from domain-wall motion. In the case of terpolymer, it could also be crystallites' orientation in the amorphous matrix.

V. CONCLUSION

In this work, we conduct simultaneous strain-polarization measurements in P(VDF-TrFE-CTFE) samples. The experiments show the existence of three intervals with different electrostrictive coefficients. More specifically, a higher coefficient is measured on an intermediate electric field range, between 30 and 70 V μm^{-1}. This allowed us to single out and quantify a specific electrostrictive mechanism present in this terpolymer.

In order to identify said mechanism, we perform *in situ* XRD measurements on a sample at different d biases. Three different behaviors are observed, matching those of our macroscopic strain measurements. Of particular interest, the intermediate electric field range show a change in the crystal structure as it went toward a less hexagonal symmetry.

Consequently, we ascribe the nonlinear electrostrictive response of P(VDF-TrFE-CTFE) to the so-called field-induced phase transition, already documented for this type of polymer. This mechanism only appears at sufficiently high ($>$30 V μm^{-1}) electric fields and is responsible of about 25% of the total strain at 100 V μm^{-1}.

ACKNOWLEDGMENTS

P.L. and E.D. thank FNR (Fonds National de la Recherche) for partly funding this research through the project CAMELHEAT C17/MS/11703691/Defay. Sylvie Tencé-Girault's contribution is achieved within the framework of the Industrial Chair Arkema (Arkema/CNRS-ENSAM-Cnam)

The authors have no conflict of interest.

[1] C. Vacher, V. Bornand, L. Fritsch, E. Billard, P. Papet, and A. Collet, P(VDF-TrFE) copolymer thin films for pyroelectric applications, Ferroelectrics **362**, 8 (2008).

[2] B. Gaihre, G. Alici, G. M. Spinks, and J. M. Cairney, Pushing the limits for microactuators based on electroactive polymers, J. Microelectromech. Syst. **21**, 574 (2012).

[3] J. Song, G. Zhao, B. Li, and J. Wang, Design optimization of PVDF-based piezoelectric energy harvesters, Heliyon **3**, e00377 (2017).

[4] C. Huang, R. Klein, F. Xia, H. Li, Q. M. Zhang, F. Bauer, and Z. Y. Cheng, Poly(vinylidene fluoride-trifluoroethylene) based high performance electroactive polymers, IEEE Trans. Dielectr. Electr. Insul. **11**, 299 (2004).

[5] E. Defaÿ, *Integration of Ferroelectric and Piezoelectric Thin Films* (John Wiley & Sons, Inc., London, United Kingdom, 2011).

[6] N. D. Kha Tu, M. S. Noh, Y. Ko, J. H. Kim, C. Y. Kang, and H. Kim, Enhanced electromechanical performance of P(VDF-TrFE-CTFE) thin films hybridized with highly dispersed carbon blacks, Compos. B: Eng. **152**, 133 (2018).

[7] S. Zhang, B. Neese, K. Ren, B. Chu, and Q. M. Zhang, Microstructure and electromechanical responses in semicrystalline ferroelectric relaxor polymer blends, J. Appl. Phys. **100**, 044113 (2006).

[8] H. Xu, Z. Y. Cheng, D. Olson, T. Mai, Q. M. Zhang, and G. Kavarnos, Ferroelectric and electromechanical properties of poly(vinylidene-fluoride–trifluoroethylene–chlorotrifluoroethylene) terpolymer, Appl. Phys. Lett. **78**, 2360 (2001).

[9] H. Kawai, The Piezoelectricity of Poly (vinylidene Fluoride), Jpn. J. Appl. Phys. **8**, 975 (1969).

[10] F. Li, L. Jin, Z. Xu, and S. Zhang, Electrostrictive effect in ferroelectrics: An alternative approach to improve piezoelectricity, Appl. Phys. Rev. **1**, 011103 (2014).

[11] I. Krakovský, T. Romijn, and A. Posthuma de Boer, A few remarks on the electrostriction of elastomers, J. Appl. Phys. **85**, 628 (1999).

[12] I. Katsouras, K. Asadi, M. Li, T. B. van Driel, K. S. Kjær, D. Zhao, T. Lenz, Y. Gu, P. W. M. Blom, D. Damjanovic, M. M. Nielsen, and D. M. de Leeuw, The negative piezoelectric effect of the ferroelectric polymer poly(vinylidene fluoride), Nat. Mater. **15**, 78 (2016).

[13] J. F. Capsal, M. Lallart, J. Galineau, P. J. Cottinet, G. Sebald, and D. Guyomar, Evaluation of macroscopic polarization and actuation abilities of electrostrictive dipolar polymers using the microscopic Debye/Langevin formalism, J. Phys. D: Appl. Phys. **45**, 205401 (2012).

[14] S. G. Lu, X. Chen, T. Levard, P. J. Diglio, L. J. Gorny, C. D. Rahn, and Q. M. Zhang, Large displacement in relaxor ferroelectric terpolymer blend derived actuators using Al electrode for braille displays, Sci. Rep. **5**, 1 (2015).

[15] F. Xia, Z. Y. Cheng, H. S. Xu, H. F. Li, Q. M. Zhang, G. J. Kavarnos, R. Y. Ting, G. Abdul-Sadek, and K. D. Belfield, High electromechanical responses in a poly(vinylidene fluoride-trifluoroethylene-chlorofluoroethylene) terpolymer, Adv. Mater. **14**, 1574 (2002).

[16] Q. Zhang, V. Bharti, and X. Zhao, Giant electrostriction and relaxor ferroelectric behavior in electron- irradiated poly(vinylidene fluoride-trifluoroethylene) copolymer, Science **280**, 2101 (1998).

[17] I. Chae, S. Ahmed, H. B. Atitallah, J. Luo, Q. Wang, Z. Ounaies, and S. H. Kim, Vibrational Sum frequency generation (SFG) analysis of ferroelectric response of PVDF-based copolymer and terpolymer, Macromolecules **50**, 2838 (2017).

[18] N. S. Sigamani, *Effect of carbon nanofillers on the microstructure and electromechanical properties of electroactive polymers*, Dissertation. (2015).

[19] M. R. Gadinski, Q. Li, G. Zhang, X. Zhang, and Q. Wang, Understanding of relaxor ferroelectric behavior of poly(vinylidene fluoride–trifluoroethylene–chlorotrifluoroethylene) terpolymers, Macromolecules **48**, 2731 (2015).

[20] D. Mao, B. E. Gnade, and M. A. Quevedo-Lopez, Ferroelectric properties and polarization switching kinetic of poly (vinylidene fluoride-trifluoroethylene) copolymer. Ferroelectrics (2011).

[21] F. Bargain, D. Thuau, P. Panine, G. Hadziioannou, F. Domingues Dos Santos, and S. Tencé-Girault, Thermal behavior of poly(VDF-ter-TrFE-ter-CTFE) copolymers: Influence of CTFE termonomer on the crystal-crystal transitions, Polymer **161**, 64 (2019).

[22] Q. Liu, C. Richard, and J. F. Capsal, Control of crystal morphology and its effect on electromechanical performances of electrostrictive P(VDF-TrFE-CTFE) terpolymer, Eur. Polym. J. **91**, 46 (2017).

[23] See Supplemental Material at http://link.aps.org/supplemental/10.1103/PhysRevApplied.14.044061 for complementary data on the influence of leakage current and measurement frequency, as well as the terpolymer complete XRD spectrum.

[24] L. Yang, B. A. Tyburski, F. D. Dos Santos, M. K. Endoh, T. Koga, D. Huang, Y. Wang, and L. Zhu, Relaxor ferroelectric behavior from strong physical pinning in a poly(vinylidene fluoride-co-trifluoroethylene-co-chlorotrifluoroethylene) random terpolymer, Macromolecules **47**, 8119 (2014).

[25] M. Newville, T. Stensitzki, D. B. Allen, and A. Ingargiola, LMFIT: Non-Linear Least-Square Minimization and Curve-Fitting for Python (2014).

[26] S. Ahmed, Z. Ounaies, and E. A. F. Arrojado, Electric field-induced bending and folding of polymer sheets, Sens. Actuators, A **260**, 68 (2017).

[27] N. S. Sigamani, S. Ahmed, and Z. Ounaies, Effect of Processing Conditions on the Microstructure and Electromechanical Response of P(VDF-TrFE-CTFE) Terpolymers. Asmedigitalcollection.Asme.Org; American Society of Mechanical Engineers Digital Collection (2014).

[28] L. Yang, X. Li, E. Allahyarov, P. L. Taylor, Q. M. Zhang, and L. Zhu, Novel polymer ferroelectric behavior via crystal isomorphism and the nanoconfinement effect, Polymer **54**, 1709 (2013).

[29] F. Bargain, P. Panine, F. Domingues Dos Santos, and S. Tencé-Girault, From solvent-cast to annealed and poled poly(VDF-co-TrFE) films: New insights on the defective ferroelectric phase, Polymer **105**, 144 (2016).